Journal of Power Sources 196 (2011) 3548–3552

Contents lists available at ScienceDirect

Journal of Power Sources

journal homepage: www.elsevier.com/locate/jpowsour

Short communication

A highly ordered Fe–N–C nanoarray as a non-precious oxygen-reduction catalyst for proton exchange membrane fuel cells

M. Lei[a], P.G. Li[a], L.H. Li[b], W.H. Tang[a,*]

[a] Department of Physics, Center for Optoelectronics Materials and Devices, Zhejiang Sci-Tech University, Xiasha College Park, Hangzhou 310018, China
[b] Department of Geology, Geography, and Physics, University of Tennessee at Martin, 215 Johnson EPS Bldg, Martin, TN 38238, USA

ARTICLE INFO

Article history:
Received 14 September 2010
Received in revised form
12 December 2010
Accepted 13 December 2010
Available online 21 December 2010

Keywords:
Highly ordered structure
Non-precious oxygen reduction catalyst
Performance

ABSTRACT

A highly ordered Pt-free Fe–N–C catalyst is synthesized through a hydrogen bonding-assisted self-assembly route. The catalyst has a porous structure with an average pore size of 5.5 nm and a large surface area of 416 $m^2 g^{-1}$, making it highly active in oxygen reduction. Cells assembled with the synthesized catalyst perform significantly better than those assembled with amorphous Fe–N–C cathode catalysts. The maximum powers of cells assembled from the highly ordered and amorphous catalysts are 252 and 60 mW cm^{-2}, respectively.

1. Introduction

Proton exchange membrane (PEM) fuel cells are expected to be alternative electrical sources for transportable and stationary applications because of their high power density and low operating temperature. Pt and its alloys remain the best cathode catalysts for PEM fuel cells. However, there is a strong incentive to find alternative catalysts because Pt is scarce and expensive [1–3]. The major limitation of PEM fuel cell performance is the oxygen reduction reaction (ORR). Recent intensive research efforts on reducing or replacing Pt-based electrodes in fuel cells have led to the development of new ORR electrocatalysts, including Pt-based alloys [4–6], transition metal chalcogenides [7–9], enzymatic catalysts [10], inorganic oxide composites [5,11], and conducting polymers or active carbon materials [12–14]. Non-precious catalysts based on Fe or Co ions are among the possible alternatives that have shown good performance compared to Pt. In this class of catalysts, a transition metal (usually Fe or Co) is stabilized by nitrogen species that are part of macrocycles, similar to the active sites in hemoglobin [15,16]. Nevertheless, these materials have poor stability in the fuel cell environment. To overcome their instability, more stable and active ORR catalysts have been fabricated through the pyrolysis of some organic macrocycles [17–22]. There have been debates on whether the transition metal acts as a catalyst for the formation of active sites during heat treatments or is part of the active site itself [23].

Researchers have aimed to fabricate catalysts into nano-network structures with large surface areas, high levels of activity, and excellent resistance to recombination, recrystallization, and sintering [24–26]. Some desired surfactants, such as non-ionic triblock copolymers, were used as structure-directing agents to achieve this goal through a facile self-assembly route [27–31]. In the self-assembly process, nanospheres can readily form closely packed, layered templates ranging from one to several layers on smooth support surfaces at properly diluted conditions. By utilizing the unique self-assembly characteristics of such nanospheres, we can fabricate novel catalysts with three-dimensional (3D) nano-network structures that are different from conventional nanocatalysts. In this work, we report a facile synthesis of a highly ordered Fe–N–C ORR catalyst that has an improved surface area and enhanced activity. ORR kinetics and single-cell performance toward the PEM fuel cell cathode are also studied.

2. Experimental

2.1. Synthesis of the highly ordered Fe–N–C catalyst

In the experiments, all the chemicals were purchased from Sigma–Aldrich Corporation. The highly ordered Fe–N–C catalysts were prepared as follows: First, 1 g iron phthalocyanine was dissolved in 38 g ethanol/water solution (10:9 weight ratio). Then, 2.5 g phloroglucinol and 2.5 g P123 (non-ionic triblock copolymer EO20PO70EO20) were dissolved into the mixture. After the chemicals were dissolved, 0.3 g HCl (37 wt.%) was added into the solution. The solution was stirred for half an hour until it turned

* Corresponding author. Tel.: +86 571 86843222; fax: +86 571 86843222.
E-mail address: whtang@zstu.edu.cn (W.H. Tang).

0378-7753/$ – see front matter © 2010 Elsevier B.V. All rights reserved.
doi:10.1016/j.jpowsour.2010.12.026

light pink. Subsequently, 2.6 g formaldehyde ethanol/water solution was added to the above solution. The solution turned cloudy after 30 min and phase separation occurred after 1 h. The lower portion of the solution of mainly phenol formaldehyde was applied to substrates by spin-coating at 2000 rpm. The film was cured at room temperature for 4 h and then at 100 °C overnight. The resulting ordered Fe–N–C catalyst was carbonized in a tubular furnace under a N_2 atmosphere at a heating rate of 1 °C min^{-1} from 100 to 400 °C and 5 °C min^{-1} from 400 to 800 °C, and kept at 800 °C for 2 h. As a comparison, an amorphous Fe–N–C catalyst was prepared by direct heat-treating the mixing reagents at 800 °C for 2 h. To yield a catalyst with a similar composition, phloroglucinol and formaldehyde were reacted for 1.5 h, after which phloroglucinol and P123 were added to the mixture.

2.2. Structure characterization of supports and catalysts

The small-angle X-ray diffraction (SAXRD) patterns of the samples were recorded on a Rigaku D/MAX-RB diffractometer (Cu Kα, 40 kV, 50 mA) at a counter rate of 2° min^{-1} from $2\theta = 0.7°$ to 10°. TEM images were obtained using a JEOL 2100F transmission electron microscope. Nitrogen adsorption–desorption data were obtained on a Quantachrome Autosorb-1 analyzer at 77 K. The surface area was calculated by the Brunauer–Emmett–Teller (BET) method. The pore-size distribution was derived from the isothermal adsorption curves using the Barrett–Joyner–Halenda (BJH) method. Prior to the measurements, samples were degassed for 12 h at 550 K.

2.3. ORR activity testing and fuel cell performance

Electrochemical measurements of the highly ordered Fe–N–C catalysts, amorphous Fe–N–C catalyst, and Pt/C catalyst (40 wt.%, E-Tek) were performed on a galvanostat/potentiostat (Autolab, PGSTAT30) with a three-electrode cell at room temperature. A Pt foil was used as the counter electrode, while a saturated calomel electrode (SCE, 0.241 V vs. a standard hydrogen electrode (SHE)) was used as the reference electrode and placed close to the glassy carbon electrode through a Luggin capillary. All potentials were expressed vs. a SHE. A catalyst ink was prepared using one part (by mass) of catalyst and 11 parts of 0.5 wt.% Nafion in aliphatic alcohol. After sonicating the ink, 10 μL of it were dispensed onto the glassy carbon disk to completely cover the current collector of the rotating ring-disk electrode (RRDE) with a thin film of catalyst. For activity testing, 0.5 M H_2SO_4 was used as the electrolyte. Gas was removed from the catalyst pores during an initial test sweep from 1.0 to 0 V (vs. the SHE) at 10 mV s^{-1} in the O_2-sparged electrolyte, thus allowing the pores to fill with the solution. The solution was then sparged with Ar, and five consecutive tests were run on the disk from 1.0 to 0.0 V (vs. the SHE) at 50 mV s^{-1}. A baseline for the disk was obtained by sweeping from 1.2 to 0.0–1.2 V (vs. the SHE) at 10 mV s^{-1} in the Ar-sparged solution at a rotation rate of 100 rpm. Finally, the solution was saturated with O_2 and a slow speed (10 mV s^{-1}) was used at a rotation rate of 1000 rpm. All the tests were multiplied by 5 to correct for this efficiency.

The MEAs of the single cells were prepared as follows [32]: First, catalyst inks were prepared by mixing the electrocatalyst, 5 wt.% Nafion solution (DuPont D520), and isopropyl alcohol at a weight ratio of 1:6:10 under vigorous stirring. The catalyst slurry was then screen-printed onto the GDL (TGP-060) to form an electrocatalytic layer. The anode was a 0.3 mg cm^{-2} Pt/C catalyst (40 wt.%), and the cathodes were a 0.6 mg cm^{-2} highly ordered Fe–N–C catalyst, amorphous Fe–N–C catalyst, and Pt/C catalyst. The catalyst layer was dried at 60 °C for 10 min and at 90 °C in an N_2 atmosphere for 3 min. The Nafion 112 membrane (50 μm) and electrocatalyst layers were bonded together by hot pressing under 10 MPa at 125 °C for 90 s. Single-fuel cells were assembled from the as-prepared MEAs and graphite flow field plates under a pressure of 10 MPa. The active area of the cell was 2 cm × 2 cm. H_2 and air were used as the fuel and oxidant, respectively. The flow rates of the former and latter were 300 and 2000 sccm, respectively. Cell performances were recorded by a Solartron 1260. Prior to the measurements, cells were activated by polarization at a constant current until stable performance was achieved.

Electrochemical impedance spectroscopy (EIS) of the single cells was performed with an Autolab Electrochemical station (PGSTAT30) under potentiostatic mode at a cell voltage close to OCV (i.e., 0.85–0.90 V) and an amplitude of 5 mV over a frequency range from 10 mHz to 10 kHz. Due to the more rapid reaction kinetics of the H_2 oxidation reaction on the Pt electrocatalysts compared to the O_2 reduction reaction, the cell impedance would be dominated by the cathodic impedance for the O_2 reduction reaction. The cell membrane resistance, R_E, was measured from the high-frequency intercept, and the polarization (or charge transfer) resistance, R_{ct}, was obtained from the difference between the low- and high-frequency intercepts of the impedance curves.

3. Results and discussions

3.1. Morphology and structure of the highly ordered Fe–N–C catalyst

The feasibility of the synthesis of highly ordered self-assembling carbon-based materials assisted by hydrogen bonding between hydrocarbon polymers and PEO-containing block copolymers had been previously demonstrated [33,34]. Formaldehyde and phloroglucinol are polymerized to form phenolic oligomers in the presence of HCl catalysts, and many hydroxyl (–OH) groups remain in the phenolic oligomers and iron phthalocyanine because of the stoichiometric ratio of superfluous phloroglucinol. Thus, phenolic oligomers and iron phthalocyanine with high –OH density self-assemble on the P123 surfactant between the –OH groups of hydrocarbon polymers and the PEO domains of PEO–PPO–PEO triblock copolymers. The tube-cumulated mesoporous phenolic oligomer–iron–phthalocyanine with the P123 surfactant template is formed through the hydrogen bonding between the phenolic oligomer/P123 triblock copolymer and iron phthalocyanine/P123 triblock copolymer. With the phase separation of P123, the colloidal complex forms an ordered phenolic oligomer/iron phthalocyanine framework. The template is removed by heat treatment, and iron phthalocyanine fragments (Fe–N and some content carbon) are then anchored into the walls of the highly ordered carbon framework.

Fig. 1a displays the TEM images of the highly ordered Fe–N–C catalyst. Ordered arrays with d spacing of ~8 nm and a wall thickness of ~3 nm are clearly shown. Fig. 1b shows the small-angle X-ray diffraction (SAXRD) patterns of the highly ordered Fe–N–C catalyst. The strong diffraction peak of the highly ordered Fe–N–C catalyst at the 2θ angle of ~0.8° corresponds to the (1 0 0) plane [20], revealing the existence of a mesoporous structure with a long-range order and a two-dimensional hexagonal symmetry. The d spacing values of the (1 0 0) peaks of the highly ordered Fe–N–C catalyst, which were calculated by Bragg's law $d_{100} = \lambda/2 \sin\theta$, were about 8 nm. The N_2 adsorption–desorption isotherms of the highly ordered Fe–N–C catalyst were also determined. The specific surface area calculated from the adsorption isotherms is 416 m^2 g^{-1}, which was significantly better than the value of ~250 m^2 g^{-1} obtained for conventional Pt/C electrocatalysts. The pore size distribution derived from the N_2 adsorption-desorption isotherms (Fig. 1c) represents highly ordered Fe–N–C arrays with a pore-sized peak

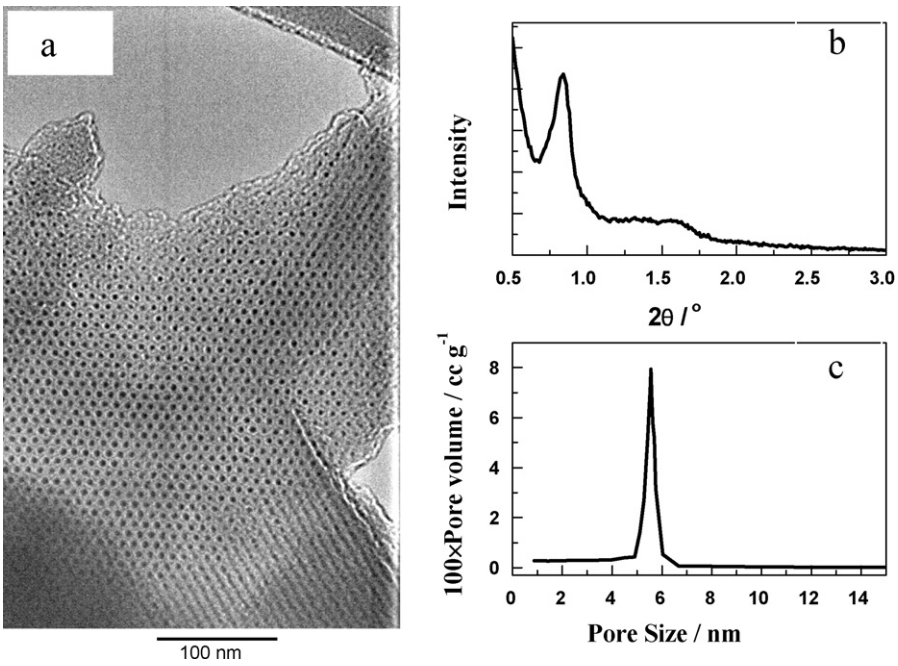

Fig. 1. (a) TEM micrograph, (b) small-angle X-ray diffraction (SAXRD) pattern, and (c) pore size distribution derived from the N_2 adsorption–desorption isotherm, of the highly ordered Fe–N–C catalyst.

centered at ~5.5 nm, consistent with the result observed from the TEM images.

XRD was conducted to obtain insights into the crystalline nature of the Fe–N/C catalysts. Fig. 2 shows the spectra of the highly ordered and amorphous Fe–N–C catalysts. As a comparison, the spectra of the Fe–N–C catalyst and the amorphous Fe–N–C catalyst before heat treatment are also displayed. Both of the samples heat-treated at 800 °C gave strong peaks at the 2θ value of 44°. These peaks can be attributed to the bulk of carbidic-state Fe and the formation of α-Fe; they have also been demonstrated to have ORR activity under acidic conditions [16,20].

3.2. ORR activity of the Fe–N–C catalyst

To optimize the heat-treatment temperature with respect to the catalytic activity, the effect of heat-treatment temperature on the catalytic ORR activity of Co–N/C catalysts was characterized using both cyclic and linear scanning voltammetry. Fig. 3(a) shows the cyclic voltammograms of Co–N/C catalysts in an N_2-saturated 0.5 M H_2SO_4 solution. No obvious oxidation or reduction current peaks were observed in the CVs, indicating that Co–N/C had no electrochemical activity over the entire potential range (0.05–1.00 V vs. the RHE). These results differ from those reported in our previous work on Fe–N/C catalysts [15,16]. Reversible redox peaks occurred at ~0.65 V (vs. the RHE) for those catalysts, and were identified as indicating the redox couple Fe(II)/Fe(III). We believe that in the potential range of 0.05–1.00 V, the Co in the Co–N/C catalyst remained as Co(II). To assess their ORR activity, the Co–N/C coated

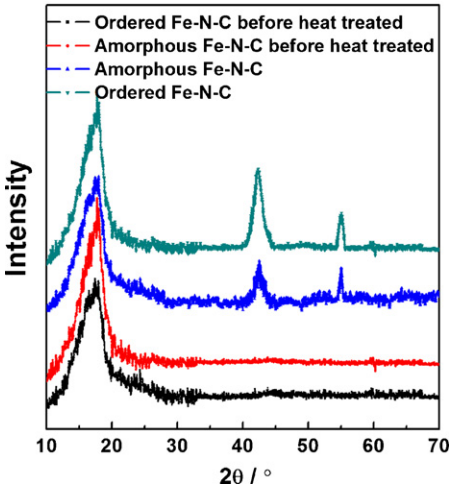

Fig. 2. XRD spectrum of the highly ordered Fe–N–C catalyst and the amorphous Fe–N–C catalyst before and after heat treated.

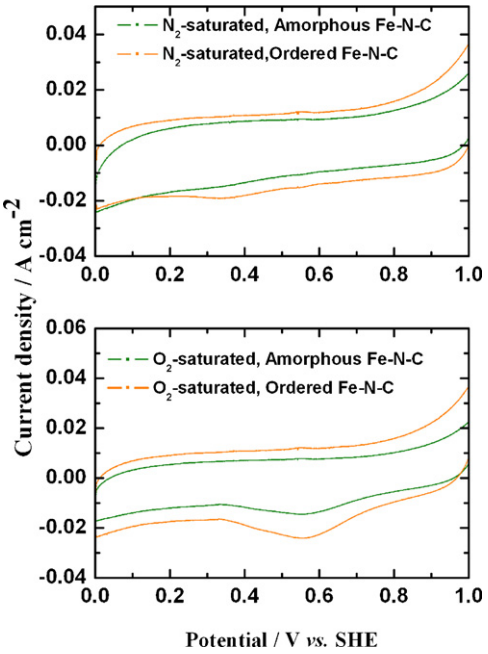

Fig. 3. Cyclic voltammograms of the highly ordered Fe–N–C catalyst and the amorphous Fe–N–C catalyst under (a) N_2-saturated and (b) O_2-saturated 0.5 M H_2SO_4 solutions.

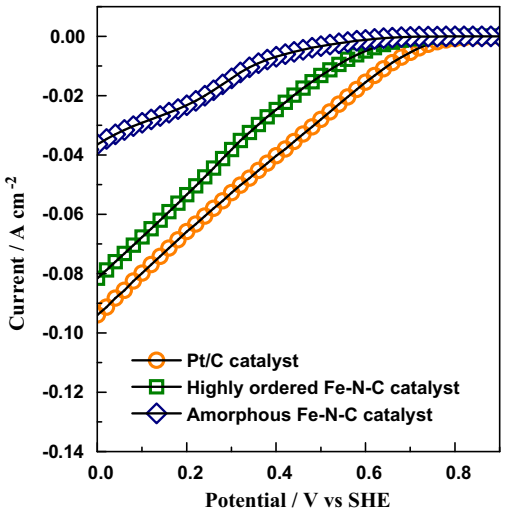

Fig. 4. ORR polarization curves of Pt/C catalyst, measured on the rotating disk electrode in 0.5 M H_2SO_4 solution saturated with O_2.

electrodes were also tested in an O_2-saturated H_2SO_4 solution. The results are shown in Fig. 3(b), where the reduction waves near 0.6 V vs. the RHE indicate that all of the catalysts were active toward the ORR. However, the different wave positions suggest that the Co–N/C catalysts obtained at different temperatures have different catalytic activities. Thus, the heat-treatment temperature has a strong effect on the ORR activity of Co–N/C catalysts. Among the Co–N/C catalysts obtained after heat treatment at 600, 700, 800, and 900 °C, the catalyst heat treated at 700 °C yielded the most positive onset potential (~0.793 V vs. the RHE) and, therefore, the best ORR activity. The inset in Fig. 3(b) shows the ORR onset potential as a function of the heat-treatment temperature, demonstrating that, among the four catalysts, the Co–N/C catalyst treated at 700 °C exhibited the most ORR activity, while the catalyst treated at 900 °C exhibited the least.

Fig. 4 shows the ORR polarization curves of the Pt/C catalyst, highly ordered Fe–N–C catalyst and amorphous Fe–N–C catalyst measured on the rotating disk electrode in a 0.5 M H_2SO_4 solution saturated with O_2. For the amorphous Fe–N–C catalyst, the current was only 23 mA cm^{-2} at a potential of 0.2 V vs. the SHE. For the highly ordered Fe–N–C catalyst, the current was 53 mA cm^{-2} at the same potential, very close to the value of the conventional Pt/C noble catalyst (65 mA cm^{-2}). The polarization current of the highly ordered Fe–N–C catalyst for O_2 reduction at 0.2 V was more than two times higher than that of the amorphous Fe–N–C catalyst, indicating that the ordered Fe–N–C catalyst is highly electrocatalytically active for O_2 reduction reactions. The results also reveal the slightly higher onset potential of the highly ordered Fe–N–C catalyst compared to that of the amorphous Fe–N–C catalyst. While this may have resulted from the ordered structure, the specific details of such remain unclear. Nevertheless, the merits of the highly ordered Fe–N–C catalyst can be attributed mostly to the high-surface area of the catalysts generated by the ~5.5 nm ordered structure, since the surface area of pores larger than 1.5 nm was also the effective surface of the ORR [35].

3.3. Fuel cell operation of the Fe–N–C catalyst

Fig. 5a shows the polarization performance and impedance curves of single cells assembled with different cathode electrocatalysts under 100% relative humidity (RH) at 60 °C. The EIS spectra of the cells were recorded at a cell voltage of 0.7 V. Cells assembled with the highly ordered Fe–N–C catalyst demonstrated a performance that was better than that of cells assembled with the

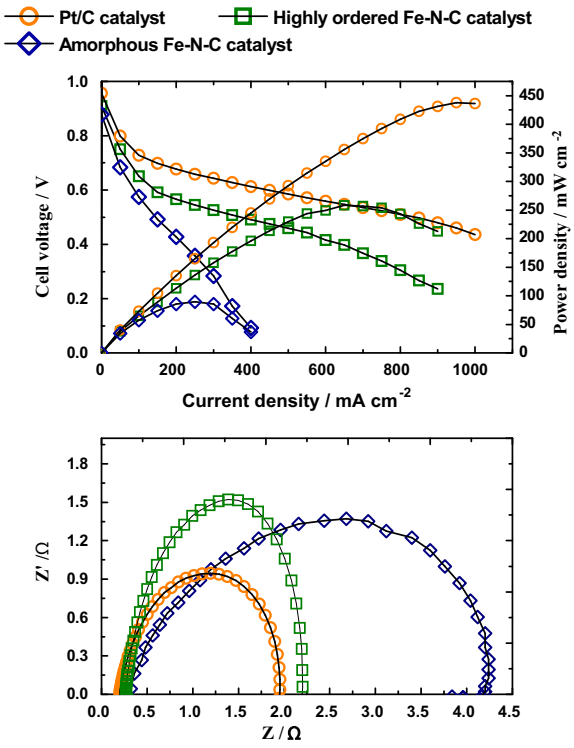

Fig. 5. (a) Polarization performance and (b) impedance spectra of single cells assembled with Pt/C catalyst, highly ordered Fe–N–C catalyst, and amorphous Fe–N–C catalyst. EIS curves were measured at a cell voltage of 0.7 V.

amorphous Fe–N–C cathode catalyst. The maximum power densities of cells assembled with the highly ordered and amorphous catalysts were 252 and 60 mW cm^{-2}, respectively. Cells assembled with the conventional noble Pt/C cathode have the highest performance. Kinetic losses are predominating at low current densities and are mainly caused by the irreversibility of the ORR reaction. In comparison with that of the noble Pt/C cathode, the curves of the Fe–N–C cathode have a higher potential loss at the kinetic control region (0–150 mA cm^{-2}), which must be contributed to the inherent lower ORR activity of the Fe–N–C catalyst. However, the performance of the Fe–N–C cathode with highly ordered structures was remarkabely improved because of the increase of active sites and the favorable mass transport of mesoporous structure. The impedance responses of the samples represent a single impedance arc over the entire frequency range, reflecting the charge transfer dominance in the electrocatalyst layer (Fig. 5b). The electrolyte resistance, R_E, for the electrode reaction under 100% RH at 60 °C ranged from 0.19 to 0.2 Ω for the cell with all cathode samples, revealing that the highly ordered Fe–N–C catalyst is highly conductive and compatible with the Nafion electrolyte interface. The cell assembled with noble Pt/C cathode displays the least R_{ct} of about 1.7 Ω, in comparison to about 2.0 Ω of the cell with the highly ordered Fe–N–C catalyst. The results suggest that the highly ordered Fe–N–C catalyst should be further improved to increase the ORR activities and meet the practical fuel cell applications. However, the validity of improving the ORR activities of the Pt-free catalyst through a high surface area and highly ordered structure was demonstrated since the highly ordered Fe–N–C catalyst have a much lower R_{ct} in contrast with the amorphous Fe–N–C catalyst. The lower performance of the cell with the amorphous Fe–N–C cathode catalyst results from its lower activity in comparison to that of the cell with the highly ordered Fe–N–C catalyst. Similar to the impedance results, the R_{ct} of the cell was about 4.1 Ω for the cells with the amorphous Fe–N–C catalyst, while that for

the cell assembled with the highly ordered Fe–N–C catalyst was about 2.0 Ω.

4. Conclusions

A highly ordered Pt-free Fe–N–C catalyst was synthesized through a hydrogen bonding-assisted, self-assembly route. The synthesized catalyst was found to have a large surface area of 416 $m^2 g^{-1}$ and an average pore size centered at about 5.5 nm. The enhanced catalyst surface area and unique structure arrangement are beneficial to the electrocatalyst and make the Pt-free catalyst highly active to oxygen reduction. Cells assembled with the highly ordered Fe–N–C catalyst have a performance that is significantly better than that of cells assembled with amorphous Fe–N–C cathode catalysts. The maximum power densities achieved by cells with the highly ordered and amorphous catalysts were 252 and 60 mW cm^{-2}, respectively. The research also demonstrated that the ordered Pt-free Fe–N–C catalyst is highly conductive and compatible to Nafion electrolyte interfaces, with a R_E of 0.2 Ω in the fuel cell operated. The high performance of the cell with highly ordered Fe–N–C catalysts results from its excellent activity in comparison to that of the cell with amorphous Fe–N–C cathode catalysts. The charge transfer resistance of the cell assembled with amorphous Fe–N–C cathode catalyst was about 4.1 Ω, while that of the cell assembled with the highly ordered Fe–N–C catalyst was about 2.0 Ω.

Acknowledgements

This work was supported by the National Basic Research Program of China (973 Program, Grant No.: 2010CB933501), the Innovative Youth Team of Natural Science Foundation of Zhejiang Province (Grant No.: R4090058), and the National Natural Science Foundation of China (Grant No. 51072182).

References

[1] L. Zhang, J.J. Zhang, D.P. Wilkinson, H.J. Wang, J. Power Sources 156 (2006) 171.
[2] B. Wang, J. Power Sources 152 (2005) 1.
[3] H.A. Gasteiger, S.S. Kocha, B. Sompalli, F.T. Wagner, Appl. Catal. B Environ. 56 (2005) 9.
[4] V.R. Stamenkovic, B. Fowler, B.S. Mun, G.F. Wang, P.N. Ross, C.A. Lucas, N.M. Markovic, Science 315 (2007) 493.
[5] C. Wang, H. Daimon, S.H. Sun, Nano Lett. 9 (2009) 1493.
[6] H. Meng, P.K. Shen, Electrochem. Commun. 8 (2006) 588.
[7] J.M. Ziegelbauer, D. Gatewood, A.F. Gulla, M.J.F. Guinel, F. Ernst, D.E. Ramaker, S. Mukerjee, J. Phys. Chem. C 113 (2009) 6955.
[8] J.H. Kim, A. Ishihara, S. Mitsushima, N. Kamiya, K.I. Ota, Chem. Lett. 36 (2007) 514.
[9] G. Liu, H. Zhang, J. Phys. Chem. C 112 (2008) 2058.
[10] D.A. Proshlyakov, M.A. Pressler, C. DeMaso, J.F. Leykam, D.L. DeWitt, G.T. Babcock, Science 290 (2000) 1588.
[11] Y. Okamoto, Appl. Surf. Sci. 255 (2008) 3434.
[12] M. Lefevre, E. Proietti, F. Jaouen, J.P. Dodelet, Science 324 (2009) 71.
[13] T. Iwazaki, R. Obinata, W. Sugimoto, Y. Takasu, Electrochem. Commun. 11 (2009) 376.
[14] K.P. Gong, F. Du, Z.H. Xia, M. Durstock, L.M. Dai, Science 323 (2009) 760.
[15] F. Jaouen, F. Charreteur, J.P. Dodelet, J. Electrochem. Soc. 153 (2006) A689.
[16] C.W.B. Bezerra, L. Zhang, K.C. Lee, H.S. Liu, A.L.B. Marques, E.P. Marques, H.J. Wang, J.J. Zhang, Electrochim. Acta 53 (2008) 4937.
[17] A.H.C. Sirk, S.A. Campbell, V.I. Birss, J. Electrochem. Soc. 155 (2008) B592.
[18] R. Bashyam, P. Zelenay, Nature 443 (2006) 63.
[19] H.S. Liu, C.J. Song, Y.H. Tang, J.L. Zhang, H.J. Zhang, Electrochim. Acta 52 (2007) 4532.
[20] C.W.B. Bezerra, L. Zhang, K.C. Lee, H.S. Liu, J.L. Zhang, Z. Shi, A.L.B. Marques, E.P. Marques, S.H. Wu, J.J. Zhang, Electrochim. Acta 53 (2008) 7703.
[21] A. Garsuch, R. Yang, A. Bonakdarpour, J.R. Dahn, Electrochim. Acta 53 (2008) 2423.
[22] R.Z. Yang, T.R. Dahn, J.R. Dahn, J. Electrochem. Soc. 156 (2009) B493.
[23] A. Bonakdarpour, M. Lefevre, R.Z. Yang, F. Jaouen, T. Dahn, J.P. Dodelet, J.R. Dahn, Electrochem. Solid-State Lett. 11 (2008) B105.
[24] X.Y. Zhang, W. Lu, J.Y. Da, H.T. Wang, D.Y. Zhao, P.A. Webley, Chem. Commun. (2009) 195.
[25] E.P. Lee, Z.M. Peng, D.M. Cate, H. Yang, C.T. Campbell, Y. Xia, J. Am. Chem. Soc. 129 (2007) 10634.
[26] J.L. Shui, J.C.M. Li, Nano Lett. 9 (2009) 1307.
[27] X.J. Meng, T. Kimura, T. Ohji, K. Kato, J. Mater. Chem. 19 (2009) 1894.
[28] L.A. Cao, T. Man, M. Kruk, Chem. Mater. 21 (2009) 1144.
[29] S.M. Morris, P.F. Fulvio, M. Jaroniec, J. Am. Chem. Soc. 130 (2008) 15210.
[30] Y. Huang, H.Q. Cai, T. Yu, F.Q. Zhang, F. Zhang, Y. Meng, D. Gu, Y. Wan, X.L. Sun, B. Tu, D.Y. Zhao, Angew. Chem. Int. Ed. 46 (2007) 1089.
[31] P.D. Yang, D.Y. Zhao, B.F. Chmelka, G.D. Stucky, Chem. Mater. 10 (1998) 2033.
[32] H.L. Tang, S.L. Wang, S.P. Jiang, M. Pan, J. Power Sources 170 (2007) 140–144.
[33] A.T. Rodriguez, X.F. Li, J. Wang, W.A. Steen, H.Y. Fan, Adv. Funct. Mater. 17 (2007) 2710–2716.
[34] C.D. Liang, S. Dai, J. Am. Chem. Soc. 128 (2006) 5316.
[35] D. Qu, Carbon 45 (2007) 1296.